Hindawi Publishing Corporation
Advances in Materials Science and Engineering
Volume 2012, Article ID 905474, 13 pages
doi:10.1155/2012/905474

Review Article

Radiation Effects in Nuclear Ceramics

L. Thomé,[1] S. Moll,[1] A. Debelle,[1] F. Garrido,[1] G. Sattonnay,[2] and J. Jagielski[3,4]

[1] *Centre de Spectrométrie Nucléaire et de Spectrométrie de Masse, CNRS/IN2P3 et Université Paris-Sud, Bât. 108, 91405 Orsay, France*
[2] *LEMHE/ICMMO, UMR 8182, Université Paris-Sud, Bât. 410, 91405 Orsay, France*
[3] *Institute for Electronic Materials Technology, Wolczynska 133, 01-919 Warsaw, Poland*
[4] *The Andrzej Soltan Institute for Nuclear Studies, 05-400 Swierk/Otwock, Poland*

Correspondence should be addressed to L. Thomé, thome@csnsm.in2p3.fr

Received 29 March 2011; Accepted 17 May 2011

Academic Editor: Robert G. Elliman

Due to outstanding physicochemical properties, ceramics are key engineering materials in many industrial domains. The evaluation of the damage created in ceramics employed in radiative media is a challenging problem for electronic, space, and nuclear industries. In this latter field, ceramics can be used as immobilization forms for radioactive wastes, inert fuel matrices for actinide transmutation, cladding materials for gas-cooled fission reactors, and structural components for fusion reactors. Information on the radiation stability of nuclear materials may be obtained by simulating the different types of interactions involved during the slowing down of energetic particles with ion beams delivered by various types of accelerators. This paper presents a review of the radiation effects occurring in nuclear ceramics, with an emphasis on recent results concerning the damage accumulation processes. Energetic ions in the KeV-GeV range are used to explore the nuclear collision (at low energy) and electronic excitation (at high energy) regimes. The recovery by electronic excitation of the damage created by ballistic collisions (SHIBIEC process) is also addressed.

1. Introduction

Ceramics are key engineering materials in many domains of human activity due to outstanding physicochemical properties, such as high strength, low-thermal expansion, chemical stability, and good behavior under irradiation. Therefore, these materials are often employed in hostile media where efficient use of energy is a prime need, for example, extreme temperatures, corrosive surroundings, and radiative environment. Industrial applications concern electronic, space, and nuclear fields. For instance, ceramics are nowadays widely used for surface coating and electronic packaging, and they are envisioned in a near future as immobilization forms for radioactive wastes, inert fuel matrices for actinide transmutation, cladding materials for gas-cooled fission reactors, and structural components for fusion reactors. In most of these applications, there is an urgent need of data for a fundamental understanding of the processes of radiation damage.

Information on the radiation stability of nuclear materials may be gained by simulating the different types of interactions (nuclear and electronic) involved during the slowing down of energetic particles with ion beams delivered by various types of low-, medium-, and high-energy accelerators. A rather broad panoply of advanced techniques (e.g., Rutherford backscattering spectrometry in channeling conditions (RBS/C), X-ray diffraction (XRD), transmission electron microscopy (TEM), and Raman spectroscopy), which sense the investigated materials at various spatial scales and with different sensitivities, can be implemented to (i) monitor the damage buildup, (ii) quantify the strain/stress level as a function of ion fluence, (iii) characterize radiation defects, (iv) determine the formation of new phases, (v) specify the parameters which trigger the (micro)structural changes, and (vi) understand the mechanisms involved in the damage formation. Results may then feed databases, be compared to computational works (using for instance molecular dynamics tools), and finally help the development of theoretical models or at least of phenomenological descriptions.

The topic that is concerned here is extremely broad. A huge number of papers were published in the last three decades on the damage production in nuclear materials, and

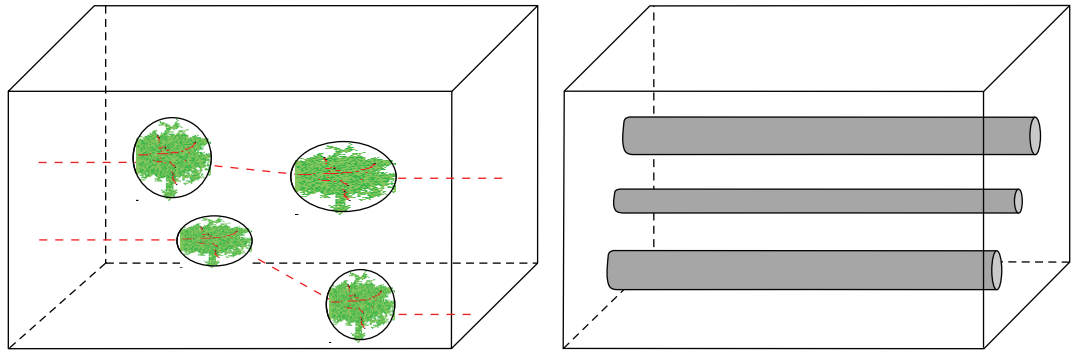

Figure 1: Schematic representation of the damage topology in crystals irradiated with slow (a) or swift (b) ions.

the state of knowledge was regularly upgraded in thorough reviews (see for instance, [1–10]). To deal the subject in a rather short article, we focus our presentation on a few remarkable examples concerning the ion-beam modifications of selected nuclear ceramics, namely, zirconia, urania, spinels, pyrochlores, and silicon carbide, with an emphasis on the damage buildup, the quantification of the strain/stress level, and the determination of the nature of radiation defects. We report results obtained by performing ion irradiation in a broad energy range (from KeV to GeV) in order to explore both nuclear collision (slow ions) and electronic excitation (swift ions) regimes, as well as synergies between the two types of processes.

Section 2 is devoted to the presentation of general considerations about the damage accumulation processes in ion-irradiated materials and to the description of models developed to interpret experimental results. The effects of elastic collisions generated by slow ions and electronic excitations induced by swift ions are addressed in Sections 3 and 4. The last section presents a new phenomenon, due to a synergetic effect between nuclear and electronic interactions, which consists in the recrystallization by electronic excitation of the defective microstructure produced upon ballistic collisions.

2. Models of Damage Accumulation

The topology of the damage resulting from irradiation of a crystal with low- or high-energy ions is schematically represented in Figure 1. For slow ions (i.e., below ~10 KeV/u), the basic process of ion energy loss is the direct transfer of energy to the atoms of the solid by elastic collisions between the projectile and the target nuclei (S_n). Along the ion path, a large fraction of primary knock-on atoms set in motion by incident ions gain a sufficient amount of energy to subsequently displace other target atoms through several secondary and higher-order collisions. These ballistic processes lead to the creation of damage cascades [11] which are represented by the ovoid objects in Figure 1(a). For swift ions (i.e., above ~1 MeV/u), the electronic energy deposition (S_e) induces the formation of electrostatically unstable cylinders of ionized atoms, called latent track [12], which are represented by the grey objects in Figure 1(b). The resulting atomic rearrangements may be interpreted in the framework of thermal spike [13–16] or Coulomb explosion [17–19] mechanisms.

The first description of the damage buildup in ion-irradiated crystals was provided by Gibbons [20] which assumed that the radiation-induced damage accumulation (quantified by the parameter f_D) is due to the overlapping of a number m of ion impacts in a given volume of a target, according to the equation:

$$f_D = f_D(\infty)\left[1 - \sum_{k=0}^{m-1} \frac{(\sigma_G \Phi)^k}{k!} \exp(-\sigma_G \Phi)\right], \quad (1)$$

where $f_D(\infty)$ is the value of f_D at saturation ($f_D = 1$ in the case where the final state is amorphous) and σ_G is the disordering cross-section. More sophisticated models (see [6]) were then elaborated to account for the experimentally determined damage buildups with more or less complicated shapes. These models are based on a combination of direct-impact and damage-accumulation descriptions with the possibility of considering additional processes such as cascade-overlap, interface-controlled, and defect-stimulated mechanisms.

Another model, referred to as MSDA for multistep damage accumulation [23], which has been recently improved [24], was developed to circumvent a number of drawbacks revealed in previous descriptions. This model is based on the hypothesis that the radiation damage results from a series of successive atomic reorganizations (steps) which are triggered by microscopic or macroscopic solicitations, so that the damage accumulation follows the equation:

$$f_D = \sum_{i=1}^{n-1} \left\{ f_{D,i}^{\text{sat}} G[1 - \exp(-\sigma_i(\Phi - \Phi_i))] \times \prod_{k=1}^{i-1} [\exp(-\sigma_{i+1}(\Phi - \Phi_{i+1}))] \right\} + f_{D,n}^{\text{sat}} G[1 - \exp(-\sigma_n(\Phi - \Phi_n))], \quad (2)$$

where n is the number of steps required for the achievement of the total process, $f_{D,i}^{\text{sat}}$ is the level of damage at saturation,

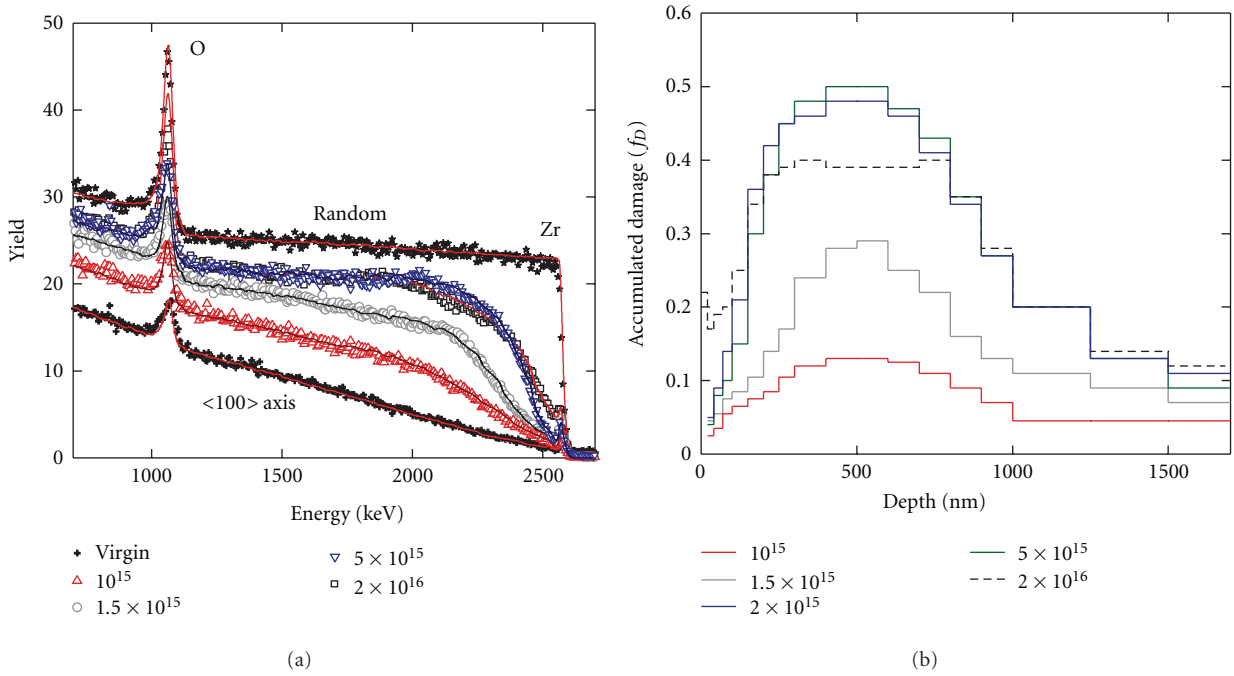

(a) (b)

FIGURE 2: (a) RBS spectra recorded on cubic zirconia crystals irradiated at RT with 4-MeV Au ions in random (stars) and ⟨100⟩-aligned (other symbols) directions (ion fluences are given in cm^{-2}). Energy of analyzing He beam: 3.07 MeV. Solid lines are fits to experimental data with the McChasy code [21, 22]. (b) Accumulated damage (f_D) as a function of depth extracted from the fits to experimental RBS data for cubic zirconia crystals irradiated with 4-MeV Au ions at the indicated fluences.

σ_i is the cross-section for damage formation, and Φ_i is the threshold irradiation fluence, for the ith step. G is a function which transforms negative values into 0 and leaves positive values unchanged.

Implementation of this model to the analysis of damage buildups obtained for ion-irradiated test-case ceramics is provided in the following two sections.

3. Effects of Elastic Collisions (Slow Ions)

Defect cascades created by low-energy ion irradiation are responsible for a large variety of (micro)structural modifications (topological or chemical disorder, swelling, phase transformations, polygonization, amorphization, etc.) which obviously depend on the target material but also on several key parameters such as the irradiation temperature, the ion fluence, flux, and energy.

The RBS/C technique is particularly well suited for the determination of damage buildups in ion-irradiated crystalline solids. An example of RBS/C spectra is provided in Figure 2(a) in the case of cubic zirconia crystals irradiated at RT with MeV heavy ions at various fluences. The spectrum registered in a random direction displays a plateau (below 2600 keV) which corresponds to the backscattering of analyzing particles from the Zr atoms of the sample, and a peak (close to 1000 keV) due to the backscattering of analyzing particles from the O atoms. It is worth noting that the O signal is enhanced by the use of the $^{16}O(^4He,^4He)^{16}O$ resonance at a 3.04-MeV He energy. The spectrum registered in the ⟨100⟩-axial direction on a virgin crystal shows the same features with a much lower backscattering yield for both the Zr and O signals due to the channeling effect. Spectra recorded in the ⟨100⟩-axial direction on irradiated crystals exhibit an increase with increasing ion fluence (at least up to $5 \times 10^{15}\,cm^{-2}$) of both the Zr and O yields due to the creation of radiation damage. A bump is clearly observed around 2100 keV, indicating that the damage is mostly located at a depth corresponding to this energy. At $2 \times 10^{16}\,cm^{-2}$, the Zr maximum yield (measured at 2100 keV) surprisingly decreases. RBS/C spectra displayed in Figure 2(a) were fitted (solid lines) by using Monte-Carlo simulations performed with the McChasy computer code [21, 22]. Calculations rely on the basic assumption that Zr and O atoms are randomly displaced from original lattice sites during irradiation. Figure 2(b) shows the variation of the fraction of displaced atoms (f_D) as a function of the depth into the sample extracted from McChasy simulations. These data correspond to the Zr sublattice, since the amount of damage created in the O sublattice may only be measured at the depth where the resonance occurs [25, 26]. For the various fluences used f_D exhibits a peak around 500 nm, with an amplitude that increases with increasing ion fluence up to $5 \times 10^{15}\,cm^{-2}$. Above this fluence (for instance at $2 \times 10^{16}\,cm^{-2}$), a clear decrease of f_D is observed.

Figure 3(a) displays θ-2θ spectra recorded in the vicinity of the (400) Bragg reflection for cubic zirconia crystals irradiated at RT with MeV heavy ions at various fluences. Note that the (logarithmic) intensity distributions are also plotted as a function of the elastic strain ($_N\varepsilon$) in the direction normal to the surface of crystals. All spectra exhibit an intense

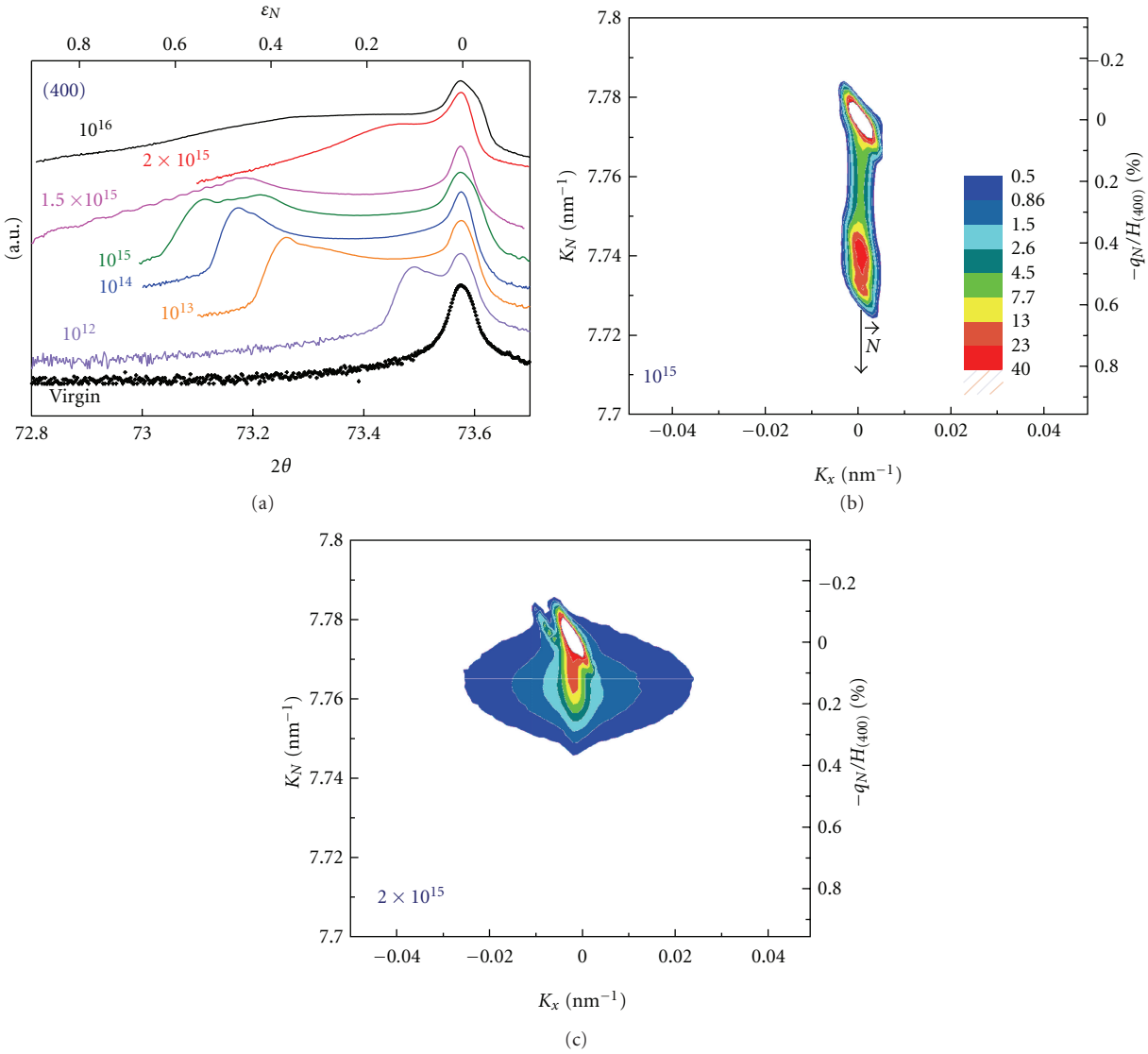

FIGURE 3: (a) θ-2θ scans recorded around the (400) reflection of cubic zirconia crystals irradiated at RT with 4-MeV Au ions. Note that the intensity is also displayed as a function of the normalized deviations from the reciprocal lattice vector $(-q_N/H_{(400)})$, which is equal to the elastic strain in the direction normal to the surface sample. ((b)-(c)) Reciprocal space maps in the vicinity of the (400) Bragg reflection for cubic zirconia irradiated at RT with 4-MeV Au ions at 10^{15} cm^{-2} (b) and 2×10^{15} cm^{-2} (c).

narrow peak on the high-angle side, corresponding to the unirradiated part of samples (since the probed thickness is higher than that of the irradiated layer), which may be taken as an internal gauge to quantify the irradiation-induced normal strain. For irradiated samples, an additional signal appears on the low-angle side (i.e., in the region of higher lattice parameter), which clearly indicates a lattice dilatation along the direction normal to the sample surface. This positive strain is induced by defects with a positive relaxation volume, most likely self-interstitial atoms. The fringe-like patterns depicted on the low-angle side indicate the presence of a nonhomogeneous strain depth distribution that can be retrieved using dedicated computer codes to fit the XRD curves [27]. However, it must be pointed out that the position of the last peak on the low-angle side of the diffraction spectra provides a good approximation of the maximum normal strain magnitude exhibited by the irradiated layer. Figures 3(b) and 3(c) show the distribution in the reciprocal space of the X-ray scattered intensity in the vicinity of the (400) Bragg reflection for samples irradiated at 10^{15} cm^{-2} (b) and 2×10^{15} cm^{-2} (c). The intensity is in logarithmic scale and the positions are located either by the in-plane (K_x) and out-of-plane (K_N) components of the scattering vector K ($2\sin\theta/\lambda$), or by the corresponding normalized deviations from the reciprocal lattice vector. On these reciprocal space maps (RSMs), a strong signal (square mesh features of the maps) is observed at the bulk theoretical coordinates. It corresponds to the unirradiated part of crystals. From this area of high intensity, the diffracted intensity spreads along the direction normal to

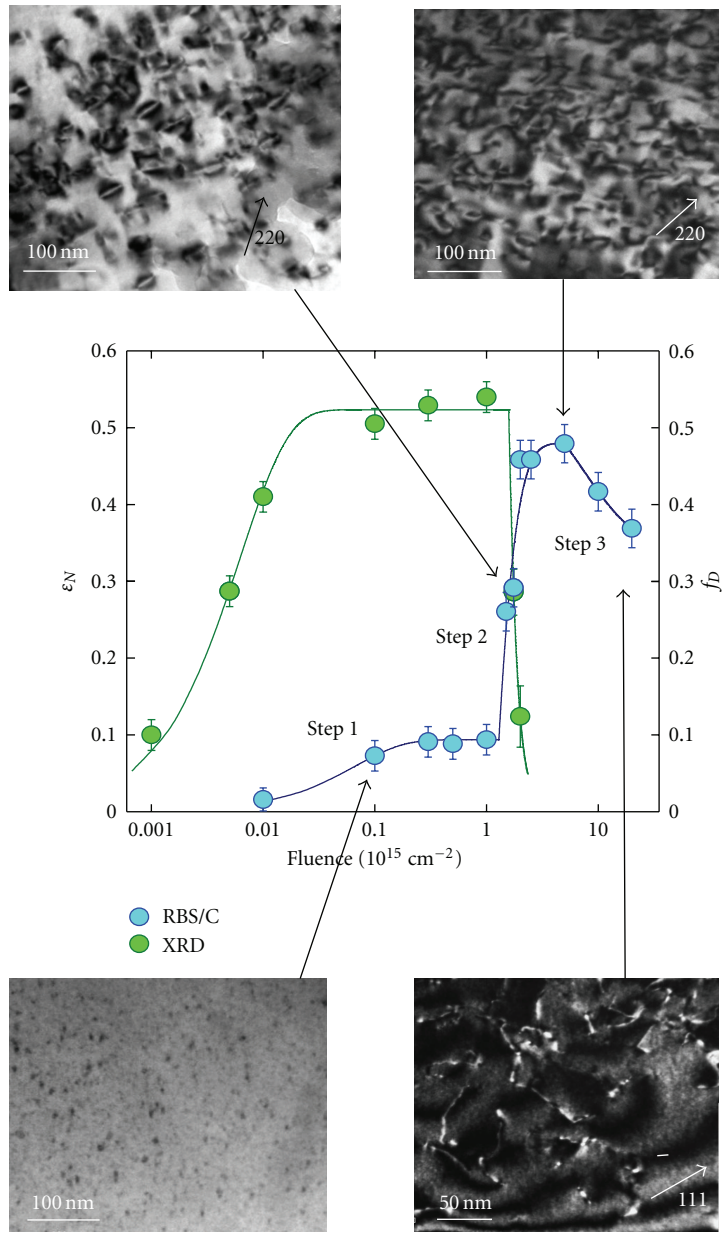

FIGURE 4: Accumulated damage (f_D) and elastic strain (ε_N) versus ion fluence for cubic zirconia crystals irradiated at RT with 4-MeV Au ions. Solid lines are fits to data using the MSDA model [23, 24]. Insets show TEM micrographs on samples irradiated at fluences indicated by the arrows.

the sample surface ($\vec{N}$) in the region of positive strain (Figure 3(b)), or broadens in the K_x direction (Figure 3(c)). The spreading along K_N, which is particularly strong for the crystal irradiated at 10^{15} cm^{-2}, indicates (as observed for the θ-2θ scans) the presence of a dilatation gradient along this direction. For this crystal, the intensity is confined in a sharp K_x region, which means that the diffuse scattering due to structural defects in the irradiated layer remains very weak. For the crystal irradiated at 2×10^{15} cm^{-2}, a strong broadening of the K_x intensity is observed in addition to a large strain relief.

Typical damage (determined by RBS/C) and strain (determined by XRD) buildups are represented in Figure 4 in the case of cubic zirconia irradiated at RT with MeV heavy ions [28]. Both sets of data may be accounted for by using the MSDA model (lines in the figure) with a value of $n = 3$ for RBS/C and $n = 2$ for XRD (where the elastic strain cannot be evaluated in step 3) in (2). TEM micrographs were recorded at typical fluences of the damage buildup (see insets of Figure 4). They indicate that (i) small defect clusters, which lead to a strong increase of the elastic strain and have a weak influence on f_D, are created during the first step (up to $\sim 10^{15}$ cm^{-2}); (ii) the second step is due to the formation of perfect dislocation loops and of a network of tangled dislocations, inducing a relaxation of the elastic strain and a sharp increase of f_D (from $\sim 10^{15}$ cm^{-2} up

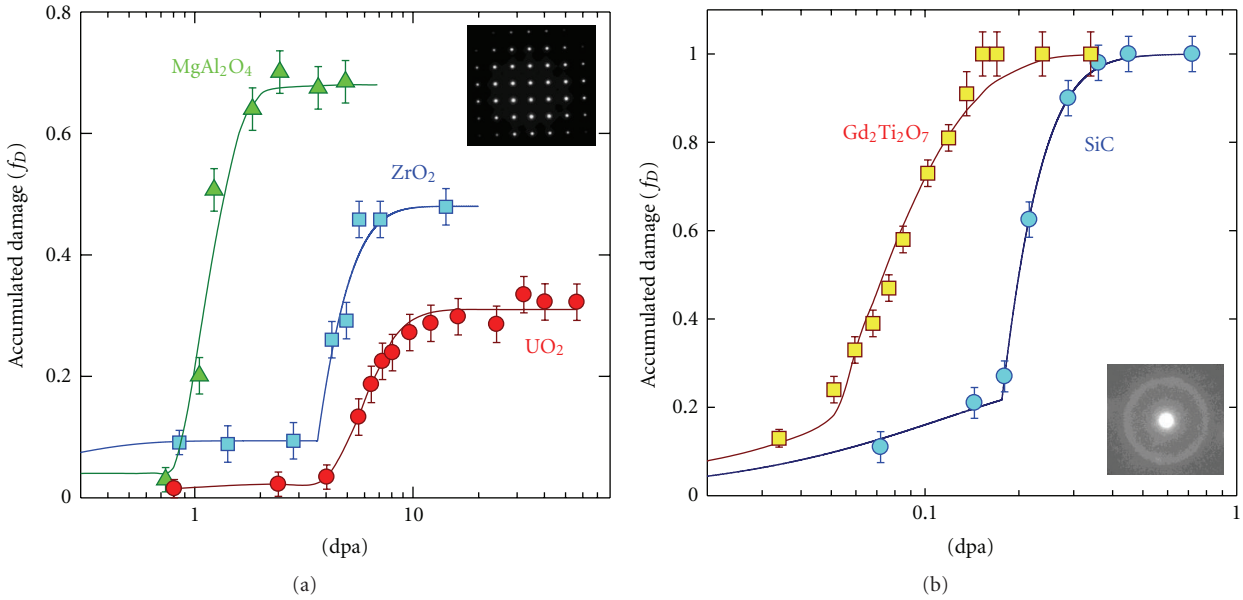

FIGURE 5: Accumulated damage (f_D) versus ion fluence for nonamorphizable (a) and amorphizable (b) ceramics irradiated at RT with slow ions. Insets show TEM diffraction patterns recorded at the final fluences on both types of materials.

to $\sim 5 \times 10^{15}\,\text{cm}^{-2}$); (iii) long dislocations, which induce a reorganization of the crystal, leading to a decrease of f_D, are exhibited in step 3 (above $\sim 5 \times 10^{15}\,\text{cm}^{-2}$). A similar behavior (except step 3) was observed in cubic zirconia irradiated with a large variety of slow ions [29], leading to the conclusion that the number of displacements per atom of the target (dpa) is the key parameter for the evolution of the damage buildup in the nuclear collision regime.

Figure 5 compares the damage buildups (expressed in dpa), as determined by RBS/C, obtained for nonamorphizable (spinel, zirconia, and urania; Figure 5(a)) and amorphizable (titanate pyrochlore and silicon carbide; Figure 5(b)) ceramics irradiated with slow ions [30–35]. It is worth mentioning that the shape of the damage kinetics may slightly differ depending on the irradiation conditions. Nevertheless, the damage accumulation process always occurs in several damage steps, so that RBS/C data may be accounted for by using the MSDA model (lines in the figure) with $n \geq 2$ in (2) for all materials. It must be noted that, except when the implanted impurities play a role in the damage process (e.g., noble gases or Cs [29]), the existence of a third step was only observed in cubic zirconia (ZrO_2) and magnesia (not shown on the figure for the sake of clarity). Nevertheless, some data at very high fluence may be missing for the observation of this third stage (for instance for $MgAl_2O_4$ and UO_2). The insets show TEM diffraction patterns recorded at the end of irradiation, which indicate that the samples either remain crystalline (Figure 5(a)) or are amorphized (Figure 5(b)) upon slow ion irradiation. It is worthwhile to mention that the value of f_D at the end of the second step of the damage accumulation cannot be taken as a reliable evaluation of the damage level in the crystal in the case of nonamorphizable materials (Figure 5(a)), since this value depends on the geometry of radiation defects via dechanneling effects inherent to the RBS/C technique. Conversely, the dose (Φ_2) at which step 2 starts, leading either to the formation of dislocation loops (in zirconia or urania) or to amorphization (in titanate pyrochlore or silicon carbide), is a parameter that can be used as an indicator of the stability of materials upon ion irradiation: the highest Φ_2, the greatest resistance to disordering or amorphization. It is worth mentioning that, for the materials selected in this study, the hierarchy is maintained irrespective of the irradiation conditions.

4. Effects of Electronic Excitation (Swift Ions)

The structure of latent tracks created in the wake of swift ions is dependent on both the ion mass (through the energy density deposited in electronic excitations) and the investigated material (insulators are generally more sensitive to S_e than semiconductors or metals).

Example of RBS/C spectra obtained for cubic zirconia crystals irradiated at RT with GeV heavy ions at various fluences is provided in Figure 6(a). Spectra registered in random and ⟨100⟩-axial directions on a virgin crystal are very similar to those shown in Figure 2(a). However, in contrast to Figure 2(a), no bump is observed around 2100 keV for spectra recorded in the ⟨100⟩-axial direction on irradiated crystals. Irradiation leads to an increase with increasing ion fluence of the Zr yield in the whole analyzed thickness, with the presence of additional disorder in the near-surface region of crystals, that is, around 2600 keV. RBS/C spectra of Figure 6(a) cannot be fitted with a simple decomposition method since they do not reveal the presence of damage peaks (as in Figure 2(a)), but rather exhibit progressive dechanneling. In such cases, the use of Monte-Carlo simulations (solid lines) performed with the McChasy

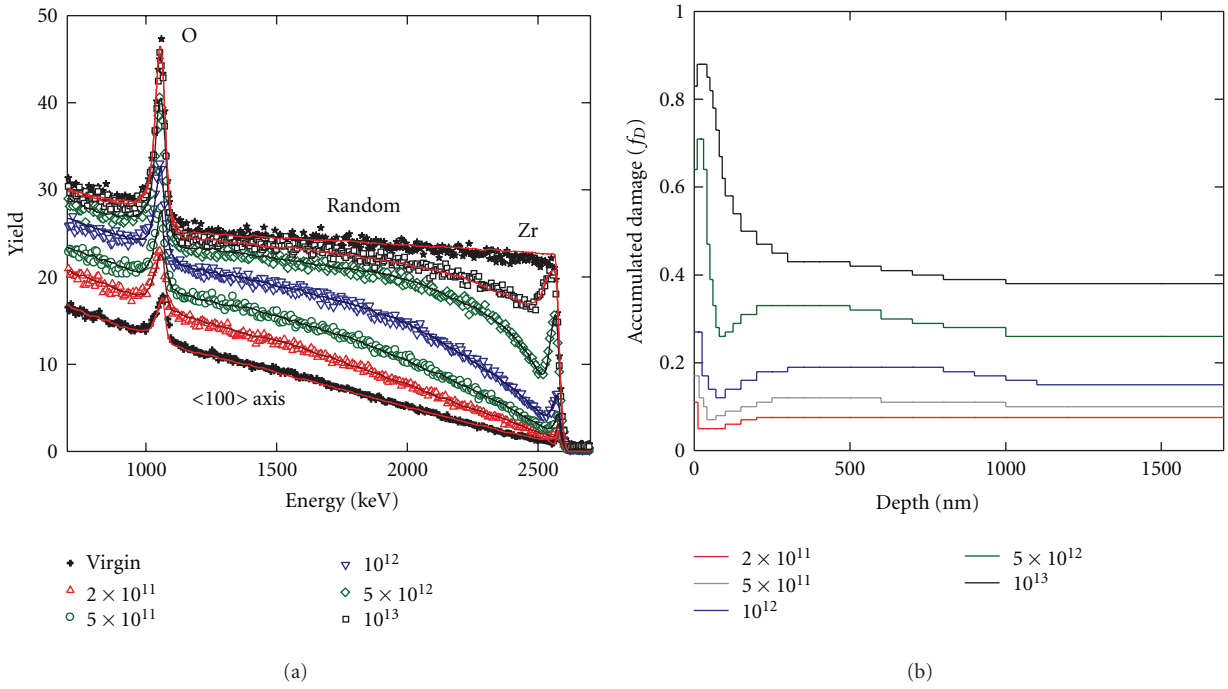

FIGURE 6: (a) RBS spectra recorded on cubic zirconia crystals irradiated at RT with 940-MeV Pb ions in random (stars) and ⟨100⟩-aligned (other symbols) directions (ion fluences are given in cm^{-2}). Energy of analyzing He beam: 3.07 MeV. Solid lines are fits to experimental data with the McChasy code [21, 22]. (b) Accumulated damage (f_D) as a function of depth extracted from the fits to experimental RBS data for cubic zirconia crystals irradiated with 940-MeV Pb ions at the indicated fluences.

computer code [21, 22] is mandatory to obtain the damage depth distributions. Here again, calculations rely on the assumption that Zr and O atoms are randomly displaced from original lattice sites during irradiation. Figure 6(b) shows the variation of the fraction of displaced atoms (in the Zr sublattice) as a function of the depth into the sample extracted from Monte-Carlo simulations. It is shown that the amount of radiation damage is almost constant with depth, except for a thin 100 nm layer below the surface where a large increase of f_D is observed. The steady value of f_D increases with increasing ion fluence, but does not exceed 0.4-0.5 at the final fluence of 10^{13} cm^{-2}.

Typical damage (determined by RBS/C) and strain (determined by XRD) buildups are represented in Figure 7 for cubic zirconia irradiated with GeV heavy ions [36]. Both sets of data may be interpreted in the framework of the MSDA model (lines in the figure) with $n = 1$ in (2). TEM micrographs, recorded at typical fluences (see the insets of Figure 7), indicate that (i) tracks are created at low fluences (below $\sim 10^{12}$ cm^{-2}); (ii) dislocation loops are formed at higher fluences (around 5×10^{12} cm^{-2}) due to the overlapping of individual ion tracks; (iii) the final microstructure at very high fluences (10^{13} cm^{-2}) is the formation of a dense network of dislocations. It is worth noting that a S_e threshold for track formation depending on the material and on the ion velocity (around 20–30 KeV/nm in cubic zirconia) was found in experiments using swift heavy ions of different masses and energies [36].

Figure 8 indicates that a single-step damage accumulation process ($n = 1$ in (2)) is also observed for other non-amorphizable (spinel and urania; Figure 8(a)) and amorphizable (titanate pyrochlore; Figure 8(b)) ceramics irradiated with swift heavy ions [37–42]. An exception is provided by silicon carbide which shows a very different response to ballistic collisions as compared to electronic excitations, since it is obviously amorphizable by the former process (see Figure 5(b)) and very weakly damaged by the latter one (see Figure 8(b)) [43]. This peculiar behavior is discussed in the next section.

Figure 9 provides the demonstration that amorphization of titanate pyrochlore occurs via the formation of amorphous tracks observed on cross-sectional (Figure 9(a)) or plane-view (Figure 9(b)) TEM micrographs. It is worth mentioning that the mean diameter of the ion tracks exhibited in Figure 9 ($d \sim 6$-7 nm) is in agreement with the diameter calculated from the damage cross-section derived from the application of the MSDA model to RBS/C data ($d = 8$ nm) [44]. The fact that the thickness of the amorphized layer is well correlated to the S_e profile is evidenced by Raman results shown in Figure 10 [45]. The vibrational mode (at 770 cm^{-1}) related to the amorphous phase is clearly seen from the surface of the sample up to a depth of ~ 20 μm (Figure 10(a)), in agreement with the S_e depth distribution obtained with the SRIM code (Figure 10(b)). In this compound, irradiations with swift ions of different masses and energies also revealed the existence of a S_e

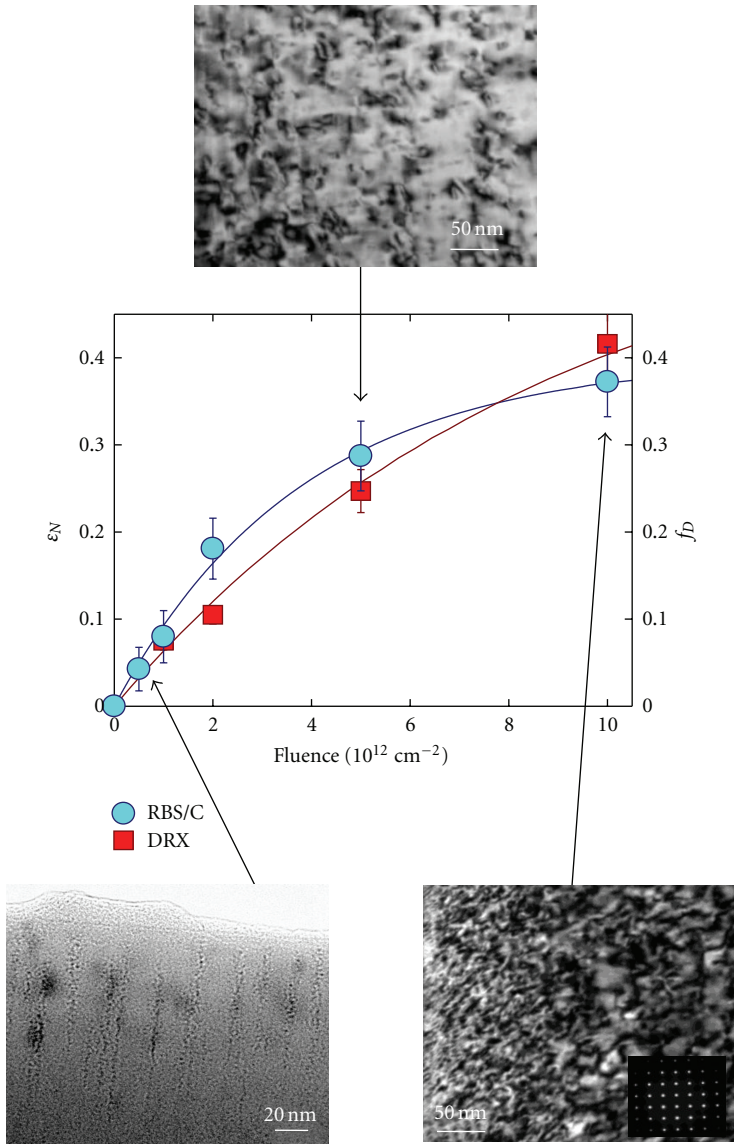

FIGURE 7: Accumulated damage (f_D) and elastic strain (ε_N) versus ion fluence for cubic zirconia crystals irradiated at RT with 940-MeV Pb ions. Solid lines are fits to data using the MSDA model [23, 24]. Insets show TEM micrographs on samples irradiated at fluences indicated by the arrows.

threshold for amorphous track formation of the order of 10 KeV/nm [45].

5. Combined Effect of Nuclear and Electronic Processes (SHIBIEC)

In previous sections it was shown that nuclear collisions induced by slow heavy ions can lead to the amorphization of irradiated layers in crystals for which electronic excitation is inefficient to produce damage (for instance SiC). In these materials, different approaches can be implemented in order to maintain or restore the crystalline structure. To prevent amorphization, the irradiation temperature can be increased above a given threshold (which is of the order of 250°C in SiC) [46–52]. Annealing of irradiation-induced amorphized samples at elevated temperatures (higher than 1000°C in SiC) [48, 50, 53, 54] induces recrystallization. Another original route lies in the use of ion-beam-induced epitaxial recrystallisation effect [55–57]. This latter methodology, generally referred to as IBIEC, consists in bombarding samples with ion species having an energy such that the slowing down is still dominated by nuclear collisions, but with an ion projected range quite deeper than the thickness of the amorphous layer. An interesting feature of IBIEC in SiC is that it occurs around 300°C [58–60], which is a quite lower temperature than that required for damage recovery by conventional thermal annealing. Recently, more energetic ion beams (GeV range) were used to recrystallize amorphous layers via the so-called swift-heavy-ion-beam-induced expitaxial crystallization (SHIBIEC) process [43, 61]. SHIBIEC does not imply the same mechanisms as

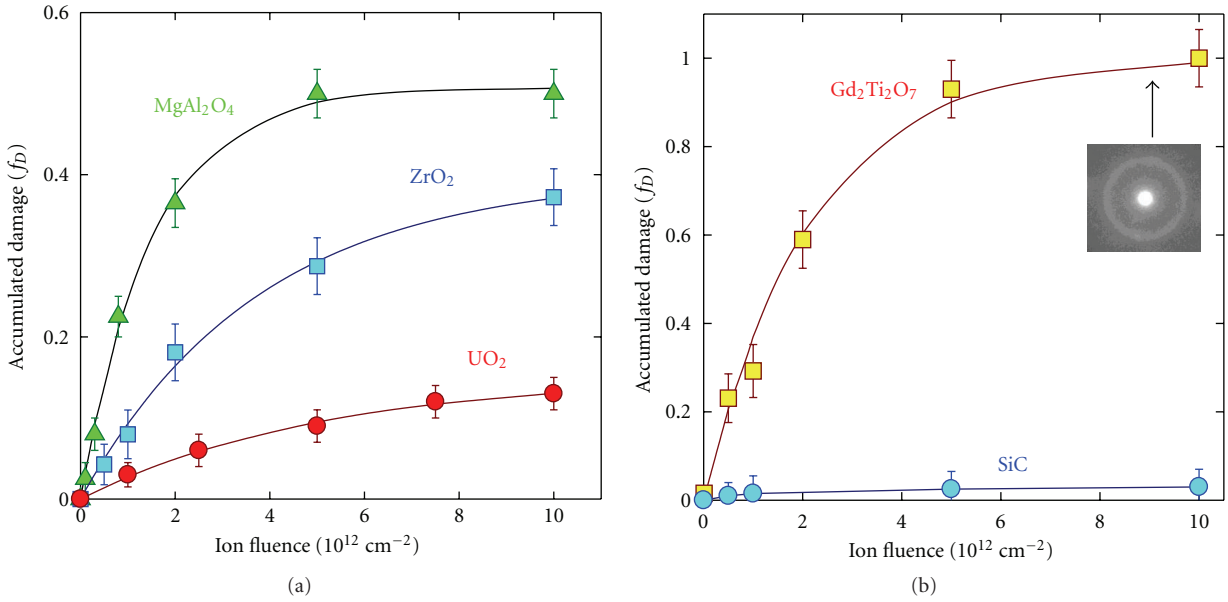

FIGURE 8: Accumulated damage (f_D) versus ion fluence for nonamorphizable (a) and amorphizable (b) ceramics irradiated at RT with swift ions. The inset shows a TEM diffraction pattern recorded at the final fluence on $Gd_2Ti_2O_7$.

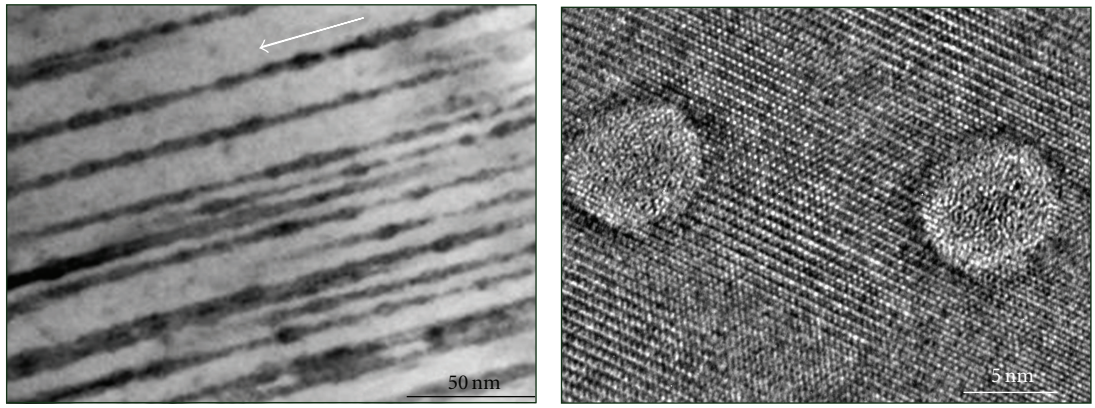

FIGURE 9: TEM micrographs recorded on a $Gd_2Ti_2O_7$ crystal irradiated at RT with 870 MeV Xe ions at 2×10^{11} cm^{-2}. (a) Cross-section; (b) plane view with a higher magnification.

those prevailing during IBIEC at low energy, but seems to be more efficient in that sense that the temperature at which recrystallization occurs is lowered as compared to that required for IBIEC.

A SHIBIEC experiment generally involves two sequences: (i) preirradiation with slow ions leading to the progressive formation of a shallow amorphous layer; (ii) postirradiation with swift ions inducing epitaxial recrystallization by electronic energy loss of the layer which was previously amorphized by nuclear collisions. Figure 11 shows an example of SHIBIEC monitored by RBS/C in the case of silicon carbide [62]. Irradiation of SiC crystals with slow Fe ions leads to the formation of an amorphous layer (the aligned signal reaches the random level: Figure 11(a)) in a 20–40 nm depth range (Figure 11(b)). Subsequent irradiation of the same sample with swift Pb ions induces a decrease of the aligned yield with increasing ion fluence (Figure 11(a)), which indicates a partial recrystallization of the amorphized layer (see also the decrease of f_D in Figure 11(b)). Results are summarized in Figure 12 that shows (i) the amorphization buildup due to slow Fe ion irradiation exhibiting a two-step process [63], and (ii) the SHIBIEC effect at different Fe fluences, which leads to a clear decrease of f_D. It is worth noting that an increase of the temperature at which swift heavy ion postirradiation is performed leads to an enhancement of the SHIBIEC process.

6. Conclusion

Energetic ions in the KeV-GeV range can be used to simulate the radiations produced in nuclear reactors or in storage forms. From a fundamental viewpoint, ion irradiations allow

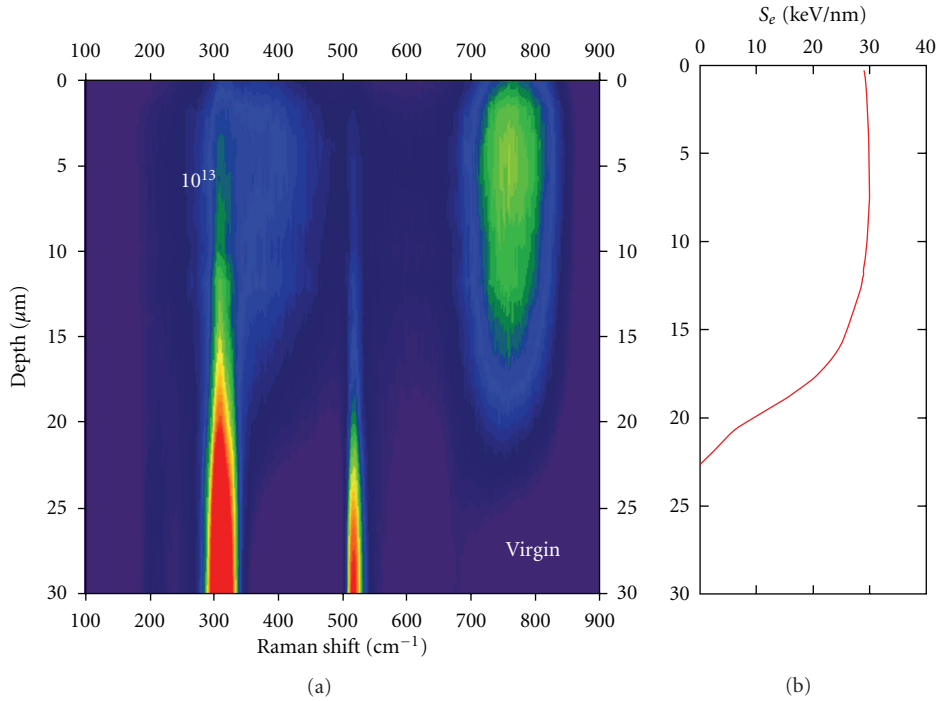

FIGURE 10: (a) Raman cartography made of spectra recorded at different depths on a $Gd_2Ti_2O_7$ crystal irradiated at RT with GeV Xe ions at 10^{13} cm^{-2}. (b) Variation with depth of the electronic energy loss (S_e) for GeV Xe ions in $Gd_2Ti_2O_7$.

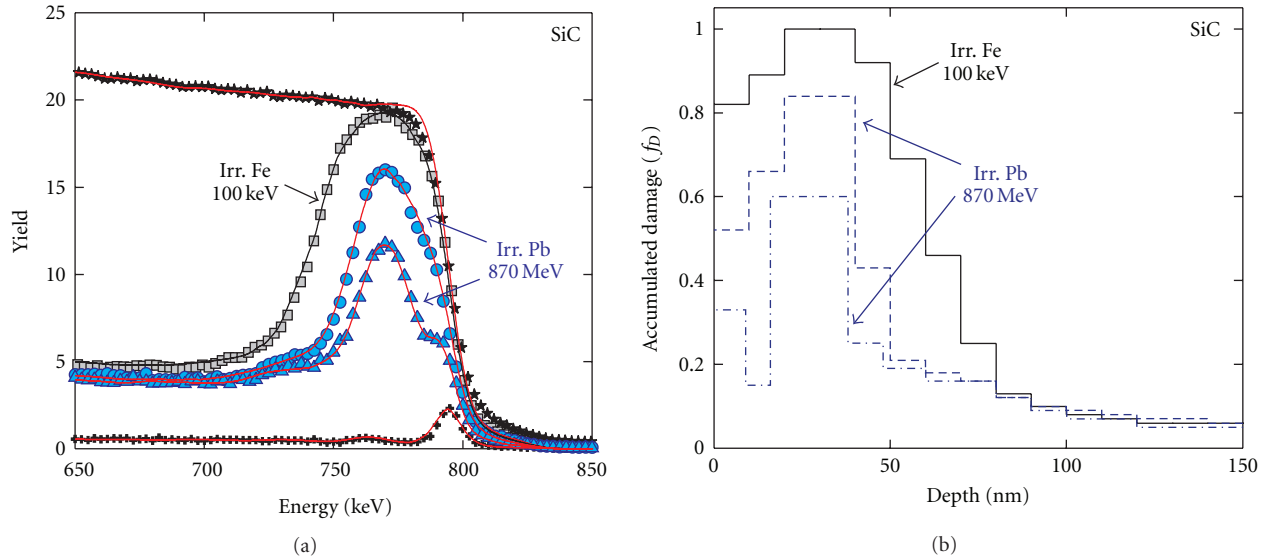

FIGURE 11: (a) RBS spectra recorded on silicon carbide crystals irradiated at RT with 100-KeV Fe ions (grey squares) and subsequently irradiated at RT with 870-MeV Pb ions (blue symbols) at 7.5×10^{12} cm^{-2} (circles) and 2×10^{13} cm^{-2} (triangles). Energy of analyzing He beam: 1.4 MeV. Solid lines are fits to experimental data with the McChasy code [21, 22]. (b) Accumulated damage (f_D) as a function of depth extracted from the fits to experimental RBS data for silicon carbide crystals irradiated at RT with 100-KeV Fe ions (black line) and subsequently irradiated at RT with 870-MeV Pb ions (blue lines) at 7.5×10^{12} cm^{-2} (dashed line) and 2×10^{13} cm^{-2} (dash-dotted line).

exploring separately the nuclear collision (at low energy) and electronic excitation (at high energy) regimes. The damage accumulation processes are generally well interpreted in the framework of the multistep damage accumulation (MSDA) model, with a number of steps strongly depending on whether nuclear collisions or electronic excitations are the dominant processes.

For slow ion irradiation, the damage depth distributions are consistent with the nuclear energy deposition. The defect cascades created by nuclear collisions lead to several steps of disorder accumulation, due to the development and relaxation of radiation-induced (mechanical) stresses. A sharp increase of the damage is most often exhibited in the second step, associated to the creation of either dislocations for

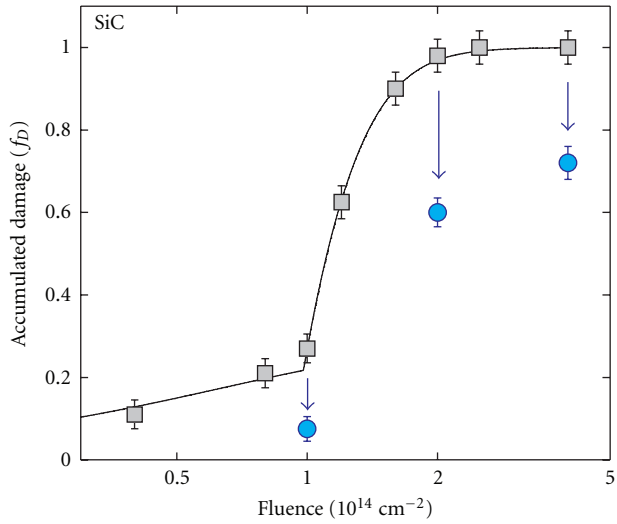

FIGURE 12: Accumulated damage (f_D) versus ion fluence for silicon carbide crystals irradiated at RT with 100 keV Fe ions (squares), and subsequently irradiated at RT (at 2×10^{13} cm^{-2}) with 870 MeV Pb ions (circles). The solid line is a fit to Fe irradiation data using the MSDA model [23, 24].

nonamorphizable materials, or amorphous layers in the case of amorphizable materials. The dose (in dpa) at which this second step occurs may be used as an indicator of the radiation resistance of materials.

For swift ion irradiation, the damage depth distributions are consistent with the electronic energy loss. Tracks created by electronic excitation cause a direct transformation of the melt volume into a new structure via a single-step process. The overlapping of tracks at high fluences leads to the formation of either dislocations or amorphous layers. Saturation of the damage is observed at fluences at least one order of magnitude lower than those required to obtain the same amount of disorder in the case of slow ion irradiation. Results also show the existence of S_e thresholds for track formation, which depend on the materials properties.

Amorphous layers formed by slow ion irradiation can be recrystallized by swift ion irradiation (SHIBIEC). This effect differs from the well-known IBIEC process by the fact that it does not require the assistance of an external heating source. It is related to the energy deposited by the incoming ions into the target electrons and can therefore be interpreted in the framework of thermal spike models. Besides the fact that the SHIBIEC process is important from a fundamental viewpoint, it presents a crucial interest for industrial applications, particularly concerning the operating cycle of nuclear reactors of the next generations. Actually, amorphization due to irradiations with neutrons or heavy ions arising from the alpha-decay of actinides can be detrimental to the physical integrity of a material. However, a balance between amorphization and damage recovery by SHIBIEC may well occur in order to preserve the crystallinity of irradiated nuclear materials, since swift ions (i.e., fission fragments) are also generated in nuclear fuels.

The investigation of the synergy between radiation effects induced simultaneously by slow and swift ions offers interesting prospects in this research field. Such a daunting challenge is reachable by the development of dedicated new facilities able to deliver several ion beams in a unique irradiation chamber, such as the JANNUS platform recently operating in the Orsay-Saclay area.

Acknowledgments

This work was partially financed by the GNR MATINEX. The experimental program also benefited from grants provided by the French-Polish cooperation Program no. 01–104.

References

[1] Hj. Matzke, "Radiation damage in crystalline insulators, oxides and ceramic nuclear fuels," *Radiation Effects*, vol. 64, no. 1–4, pp. 3–33, 1981.

[2] L. W. Hobbs, F. W. Clinard Jr., S. J. Zinkle, and R. C. Ewing, "Radiation effects in ceramics," *Journal of Nuclear Materials*, vol. 216, pp. 291–321, 1994.

[3] R. C. Ewing, W. J. Weber, and F. W. Clinard Jr., "Radiation effects in nuclear waste forms for high-level radioactive waste," *Progress in Nuclear Energy*, vol. 29, no. 2, pp. 63–127, 1995.

[4] S. J. Zinkle and C. Kinoshita, "Defect production in ceramics," *Journal of Nuclear Materials*, vol. 251, pp. 200–217, 1997.

[5] C. J. McHargue, "Ion beam modification of ceramics," *Materials Science and Engineering A*, vol. 253, no. 1-2, pp. 94–105, 1998.

[6] W. J. Weber, R. C. Ewing, C. R. A. Catlow et al., "Radiation effects in crystalline ceramics for the immobilization of high-level nuclear waste and plutonium," *Journal of Materials Research*, vol. 13, no. 6, pp. 1434–1484, 1998.

[7] W. L. Gong, W. Lutze, and R. C. Ewing, "Zirconia ceramics for excess weapons plutonium waste," *Journal of Nuclear Materials*, vol. 277, no. 2-3, pp. 239–249, 2000.

[8] L. Thomé and F. Garrido, "Application of ion beams to nuclear waste issues: evaluation of nuclear ceramics," *Vacuum*, vol. 63, no. 4, pp. 619–626, 2001.

[9] R. C. Ewing, W. J. Weber, and J. Lian, "Nuclear waste disposal-pyrochlore ($A_2B_2O_7$): nuclear waste form for the immobilization of plutonium and "minor" actinides," *Journal of Applied Physics*, vol. 95, no. 11, pp. 5949–5971, 2004.

[10] J. Lian, L. M. Wang, K. Sun, and R. C. Ewing, "In situ TEM of radiation effects in complex ceramics," *Microscopy Research and Technique*, vol. 72, no. 3, pp. 165–181, 2009.

[11] D. A. Thompson, "High density cascade effects," *Radiation Effects*, vol. 56, no. 3-4, pp. 105–150, 1981.

[12] See the *Proceedings of the 8th International Symposium on Swift Heavy Ions in Matter (SHIM '09)*, Nuclear Instruments and Methods in Physics Research Section B, vol. 267, 2009.

[13] F. Seitz and J. S. Koehler, "Displacement of atoms during radiation," in *Solid State Physics: Advances in Research and Applications*, F. Seitz and D. Turnbull, Eds., pp. 305–448, Academic Press , New York, NY, USA, 1956.

[14] M. Toulemonde, C. Dufour, and E. Paumier, "Transient thermal process after a high-energy heavy-ion irradiation of amorphous metals and semiconductors," *Physical Review B*, vol. 46, no. 22, pp. 14362–14369, 1992.

[15] G. Szenes, "General features of latent track formation in magnetic insulators irradiated with swift heavy ions," *Physical Review B*, vol. 51, no. 13, pp. 8026–8029, 1995.

[16] H. Trinkaus and A. I. Ryazanov, "Viscoelastic model for the plastic flow of amorphous solids under energetic ion bombardment," *Physical Review Letters*, vol. 74, no. 25, pp. 5072–5075, 1995.

[17] R. L. Fleischer, P. B. Price, and R. M. Walker, "Ion explosion spike mechanism for formation of charged-particle tracks in solids," *Journal of Applied Physics*, vol. 36, no. 11, pp. 3645–3652, 1965.

[18] L. E. Seiberling, J. E. Griffith, and T. A. Tombrello, "A thermalized ion explosion model for high energy sputtering and track," *Radiation effects*, vol. 52, no. 3-4, pp. 201–210, 1980.

[19] D. Lesueur and A. Dunlop, "Damage creation via electronic excitations in metallic targets: theoretical model," *Radiation Effects and Defects in Solids*, vol. 126, p. 105, 1993.

[20] J. F. Gibbons, "Ion implantation in semiconductors—part II: damage production and annealing," *Proceedings of the IEEE*, vol. 60, no. 9, pp. 1062–1096, 1972.

[21] L. Nowicki, *Damage production in cubic zirconia irradiated with swift heavy ions*, Ph.D. thesis, The Andrzej Soltan Institute for Nuclear Studies, Warsaw, Poland, 1997.

[22] L. Nowicki, A. Turos, R. Ratajczak, A. Stonert, and F. Garrido, "Modern analysis of ion channeling data by Monte Carlo simulations," *Nuclear Instruments and Methods in Physics Research, Section B*, vol. 240, no. 1-2, pp. 277–282, 2005.

[23] J. Jagielski and L. Thomé, "Multi-step damage accumulation in irradiated crystals," *Applied Physics A*, vol. 97, no. 1, pp. 147–155, 2009.

[24] J. Jagielski and L. Thomé, "Discontinuous character of the damage build-up in the elastic collision regime," *Radiation Effects and Defects in Solids*, vol. 166, no. 5, pp. 367–372, 2011.

[25] J. R. Tesmer and M. Nastasi, Eds., *Handbook of Modern Ion Beam Materials Analysis*, Materials Research Society, Pittsburgh, Pa, USA, 1995.

[26] L. Thomé, A. Gentils, J. Jagielski, S. E. Enescu, and F. Garrido, "On the use of the $^{16}O(^4He,^4He)\ ^{16}O$ resonance for the evaluation of radiation damage in oxides," *Nuclear Instruments and Methods in Physics Research, Section B*, vol. 219-220, no. 1–4, pp. 99–104, 2004.

[27] A. Boulle and A. Debelle, "Strain-profile determination in ion-implanted single crystals using generalized simulated annealing," *Journal of Applied Crystallography*, vol. 43, no. 5, pp. 1046–1052, 2010.

[28] S. Moll, L. Thomé, G. Sattonnay et al., "Multistep damage evolution process in cubic zirconia irradiated with MeV ions," *Journal of Applied Physics*, vol. 106, no. 7, Article ID 073509, 2009.

[29] L. Thomé, J. Fradin, J. Jagielski, A. Gentils, S. E. Enescu, and F. Garrido, "Radiation damage in ion-irradiated yttria-stabilized cubic zirconia single crystals," *EPJ Applied Physics*, vol. 24, no. 1, pp. 37–48, 2003.

[30] F. Garrido, C. Choffel, J. C. Dran, L. Thomé, L. Nowicki, and A. Turos, "Structural modifications in uranium dioxide irradiated with swift heavy ions," *Nuclear Instruments and Methods in Physics Research, Section B*, vol. 127-128, pp. 634–638, 1997.

[31] S. E. Enescu, L. Thomé, A. Gentils, and T. Thomé, "High-temperature annealing behavior of ion-implanted spinel single crystals," *Journal of Materials Research*, vol. 19, no. 12, pp. 3463–3473, 2004.

[32] A. Gentils, S. E. Enescu, L. Thomé, H. Khodja, G. Blaise, and T. Thomé, "High-temperature stability of ion-implanted zirconia and spinel," *Journal of Applied Physics*, vol. 97, no. 11, Article ID 113509, 6 pages, 2005.

[33] F. Garrido, L. Vincent, L. Nowicki, G. Sattonnay, and L. Thomé, "Radiation stability of fluorite-type nuclear oxides," *Nuclear Instruments and Methods in Physics Research, Section B*, vol. 266, no. 12-13, pp. 2842–2847, 2008.

[34] A. Audren, A. Benyagoub, L. Thome, and F. Garrido, "Ion implantation of iodine into silicon carbide: influence of temperature on the produced damage and on the diffusion behaviour," *Nuclear Instruments and Methods in Physics Research, Section B*, vol. 266, no. 12-13, pp. 2810–2813, 2008.

[35] Y. Zhang, J. Jagielski, I. T. Bae et al., "Damage evolution in Au-implanted $Ho_2Ti_2O_7$ titanate pyrochlore," *Nuclear Instruments and Methods in Physics Research, Section B*, vol. 268, no. 19, pp. 3009–3013, 2010.

[36] S. Moll, L. Thomé, L. Vincent et al., "Damage induced by electronic excitation in ion-irradiated yttria-stabilized zirconia," *Journal of Applied Physics*, vol. 105, no. 2, Article ID 023512, 2009.

[37] L. Thomé, J. Jagielski, A. Gentils, L. Nowicki, and F. Garrido, "Quantitative analysis of radiation-induced disorder in spinel crystals," *Nuclear Instruments and Methods in Physics Research, Section B*, vol. 242, no. 1-2, pp. 643–645, 2006.

[38] L. Thomé, A. Gentils, J. Jagielski, F. Garrido, and T. Thomé, "Physicochemical modifications induced by ion bombardment and thermal treatments in zirconia and spinel," *Nuclear Instruments and Methods in Physics Research, Section B*, vol. 250, no. 1-2, pp. 106–113, 2006.

[39] L. Thomé, A. Gentils, J. Jagielski, F. Garrido, and T. Thomé, "Radiation stability of ceramics: test cases of zirconia and spinel," *Vacuum*, vol. 81, no. 10, pp. 1264–1270, 2007.

[40] G. Sattonnay, S. Moll, L. Thomé et al., "Heavy-ion irradiation of pyrochlore oxides: comparison between low and high energy regimes," *Nuclear Instruments and Methods in Physics Research, Section B*, vol. 266, no. 12-13, pp. 3043–3047, 2008.

[41] F. Garrido, S. Moll, G. Sattonnay, L. Thomé, and L. Vincent, "Radiation tolerance of fluorite-structured oxides subjected to swift heavy ion irradiation," *Nuclear Instruments and Methods in Physics Research, Section B*, vol. 267, no. 8-9, pp. 1451–1455, 2009.

[42] S. Moll, G. Sattonnay, L. Thomé, J. Jagielski, C. Legros, and I. Monnet, "Swift heavy ion irradiation of pyrochlore oxides: electronic energy loss threshold for latent track formation," *Nuclear Instruments and Methods in Physics Research, Section B*, vol. 268, no. 19, pp. 2933–2936, 2010.

[43] A. Benyagoub, A. Audren, L. Thomé, and F. Garrido, "Athermal crystallization induced by electronic excitations in ion-irradiated silicon carbide," *Applied Physics Letters*, vol. 89, no. 24, Article ID 241914, 2006.

[44] S. Moll, G. Sattonnay, L. Thomé et al., "Irradiation damage in Gd2Ti2O7 single crystals: ballistic vs ionization processes," *In Physics Review B*. In press.

[45] G. Sattonnay, S. Moll, L. Thomé et al., "Phase transformations induced by high electronic excitation in ion-irradiated $Gd_2(Zr_xTi_{1-x})_2O_7$ pyrochlores," *Journal of Applied Physics*, vol. 108, no. 10, Article ID 103512, 2010.

[46] W. Jiang, Y. Zhang, and W. J. Weber, "Temperature dependence of disorder accumulation and amorphization in Au-ion-irradiated 6H–SiC," *Physical Review B*, vol. 70, no. 16, Article ID 165208, pp. 1–8, 2004.

[47] E. Wendler, A. Heft, and W. Wesch, "Ion-beam induced damage and annealing behaviour in SiC," *Nuclear Instruments and Methods in Physics Research, Section B*, vol. 141, no. 1–4, pp. 105–117, 1998.

[48] L. L. Snead, S. J. Zinkle, J. C. Hay, and M. C. Osborne, "Amorphization of SiC under ion and neutron irradiation," *Nuclear Instruments and Methods in Physics Research, Section B*, vol. 141, no. 1–4, pp. 123–132, 1998.

[49] Y. Zhang, W. J. Weber, W. Jiang, C. M. Wang, A. Hallén, and G. Possnert, "Effects of implantation temperature and ion flux on damage accumulation in Al-implanted 4H–SiC," *Journal of Applied Physics*, vol. 93, no. 4, pp. 1954–1960, 2003.

[50] V. Heera, A. Mücklich, C. Dubois, M. Voelskow, and W. Skorupa, "Layer morphology and Al implant profiles after annealing of supersaturated, single-crystalline, amorphous, and nanocrystalline SiC," *Journal of Applied Physics*, vol. 96, no. 5, pp. 2841–2852, 2004.

[51] J. Slotte, K. Saarinen, M. S. Janson et al., "Fluence, flux, and implantation temperature dependence of ion-implantation-induced defect production in 4H–SiC," *Journal of Applied Physics*, vol. 97, no. 3, Article ID 033513, 7 pages, 2005.

[52] Y. Katoh, N. Hashimoto, S. Kondo, L. L. Snead, and A. Kohyama, "Microstructural development in cubic silicon carbide during irradiation at elevated temperatures," *Journal of Nuclear Materials*, vol. 351, no. 1–3, pp. 228–240, 2006.

[53] K. Yoshii, Y. Suzaki, A. Takeuchi, K. Yasutake, and H. Kawabe, "Crystallization behaviour of amorphous $Si_{1-x}C_x$ films prepared by r.f. sputtering," *Thin Solid Films*, vol. 199, no. 1, pp. 85–94, 1991.

[54] M. Ishimaru, A. Hirata, M. Naito, I. T. Bae, Y. Zhang, and W. J. Weber, "Direct observations of thermally induced structural changes in amorphous silicon carbide," *Journal of Applied Physics*, vol. 104, no. 3, Article ID 033503, 2008.

[55] I. Golecki, G. E. Chapman, S. S. Lau, B. Y. Tsaur, and J. W. Mayer, "Ion-beam induced epitaxy of silicon," *Physics Letters A*, vol. 71, no. 2-3, pp. 267–269, 1979.

[56] J. Nakata, M. Takahashi, and K. Kajiyama, "In situ self ion beam annealing of damage in Si during high energy (0.53 MeV–2.56 MeV) As^+ ion implantation," *Japanese Journal of Applied Physics*, vol. 20, no. 11, pp. 2211–2221, 1981.

[57] J. Linnros, B. Svensson, and G. Holmén, "Ion-beam-induced epitaxial regrowth of amorphous layers in silicon on sapphire," *Physical Review B*, vol. 30, no. 7, pp. 3629–3638, 1984.

[58] V. Heera, J. Stoemenos, R. Kögler, and W. Skorupa, "Amorphization and recrystallization of 6H–SiC by ion-beam irradiation," *Journal of Applied Physics*, vol. 77, no. 7, pp. 2999–3009, 1995.

[59] V. Heera, R. Kögler, W. Skorupa, and J. Stoemenos, "Complete recrystallization of amorphous silicon carbide layers by ion irradiation," *Applied Physics Letters*, vol. 67, no. 14, article 1999, 3 pages, 1995.

[60] A. Kinomura, A. Chayahara, Y. Mokuno, N. Tsubouchi, and Y. Horino, "Enhanced annealing of damage in ion-implanted 4H–SiC by MeV ion-beam irradiation," *Journal of Applied Physics*, vol. 97, no. 10, Article ID 103538, 6 pages, 2005.

[61] T. Som, B. Satpati, O. P. Sinha, and D. Kanjilal, "Swift heavy-ion-induced epitaxial crystallization of buried Si_3N_4 layer," *Journal of Applied Physics*, vol. 98, no. 1, Article ID 013532, 4 pages, 2005.

[62] L. Thomé, A. Debelle, F. Garrido, and A. Declémy, to be published.

[63] A. Debelle, L. Thomé, D. Dompoint et al., "Characterization and modelling of the ion-irradiation induced disorder in 6H–SiC and 3C–SiC single crystals," *Journal of Physics D*, vol. 43, no. 45, Article ID 455408, 2010.